Size-Dependent Two-Photon Absorption and Ultralow Optical-Limiting Response in Atomically-Thin Rhodonite

Dipanwita Mitra[a], Caique Campos de Oliveira[b], Alexey Kartsev[c,d,e], Riya Sadhukhan[a], Jayanta Kumar Sarkar[a], Alexander A. Safronov[e], Dipak Kumar Goswami[a], Gelu Costin[f], Pedro Alves da Silva Autreto[b], Chandra Sekhar Tiwary[g]*, Prasanta Kumar Datta[a]**

[a] Department of Physics, Indian Institute of Technology Kharagpur, Kharagpur 721302, India

[b] Centre for Natural and Human Sciences (CCNH), Federal University of ABC (UFABC), 09210-580, Santo André - SP, Brazil

[c] Computing Center of the Far Eastern Branch of the Russian Academy of Sciences, Khabarovsk, 680000, Russia

[d] Peoples' Friendship University of Russia – RUDN University, 6 Miklukho-Maklaya Str., Moscow 117198, Russian Federation

[e] MIREA-Russian Technological University, 119454 Moscow, Russia

[f] Department of Earth Environmental and Planetary Sciences, Rice University, Houston, TX 77005, USA

[g] Department of Metallurgical and Materials Engineering, Indian Institute of Technology Kharagpur, Kharagpur 721302, India

Keywords: Rhodonite nanoflakes, ultrafast optical nonlinearity, two-photon absorption, optical limiting, bandgap engineering

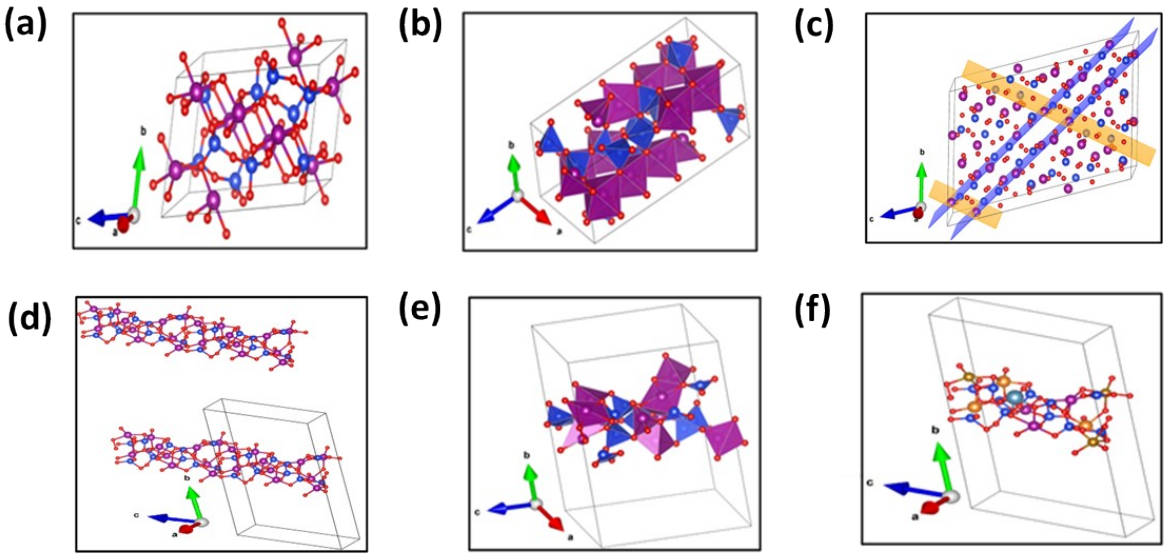

Figure S1. (a) Three- dimensional unit cell of the equilibrium structure of $MnSiO_3$. Mn ions are shown in purple, Si ions in blue, and O ions in red; (b) Bulk unit cell of the equilibrium structure of $MnSiO_3$ in the polyhedral model. The Mn-centered polyhedron is shown in purple, while the Si-centered polyhedron is in blue. Oxygen ions are positioned at the vertices of the polyhedra;(c) Supercell simulation of $MnSiO_3$. Two blue and two orange planes define the boundary of atoms included in the two-dimensional supercell of $MnSiO_3$ along the crystallographic plane; (d) Optimized supercell of quasi-two-dimensional $MnSiO_3$ in the polyhedral model. The Mn-centered polyhedron is shown in purple, and the Si-centered polyhedron in blue. Oxygen ions are located at the vertices of the polyhedral; (e) Two-dimensional layers and the unit cell of the simulated quasi-dimeric $MnSiO_3$ material; (f) Optimized supercell of quasi-two-dimensional rhodonite. Mn ions are in purple, Mg ions in orange, Fe ions in yellow, Ca ions in turquoise, Si ions in blue, and O ions in red

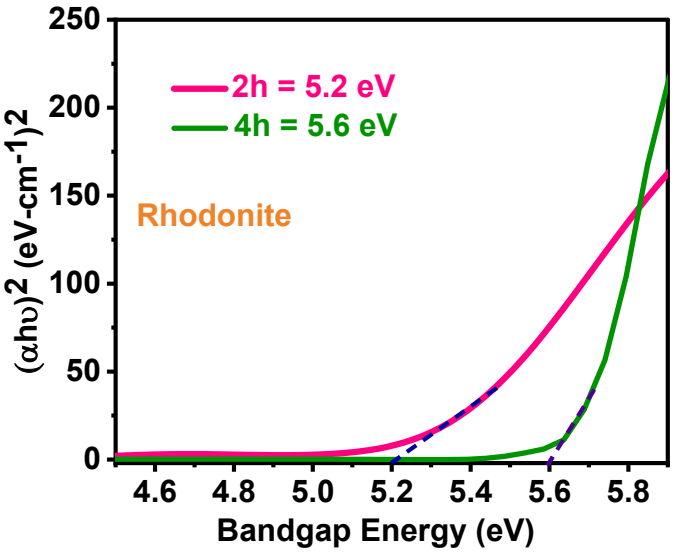

Figure S2. Optical bandgap for direct electron transition determined by Tauc plot;

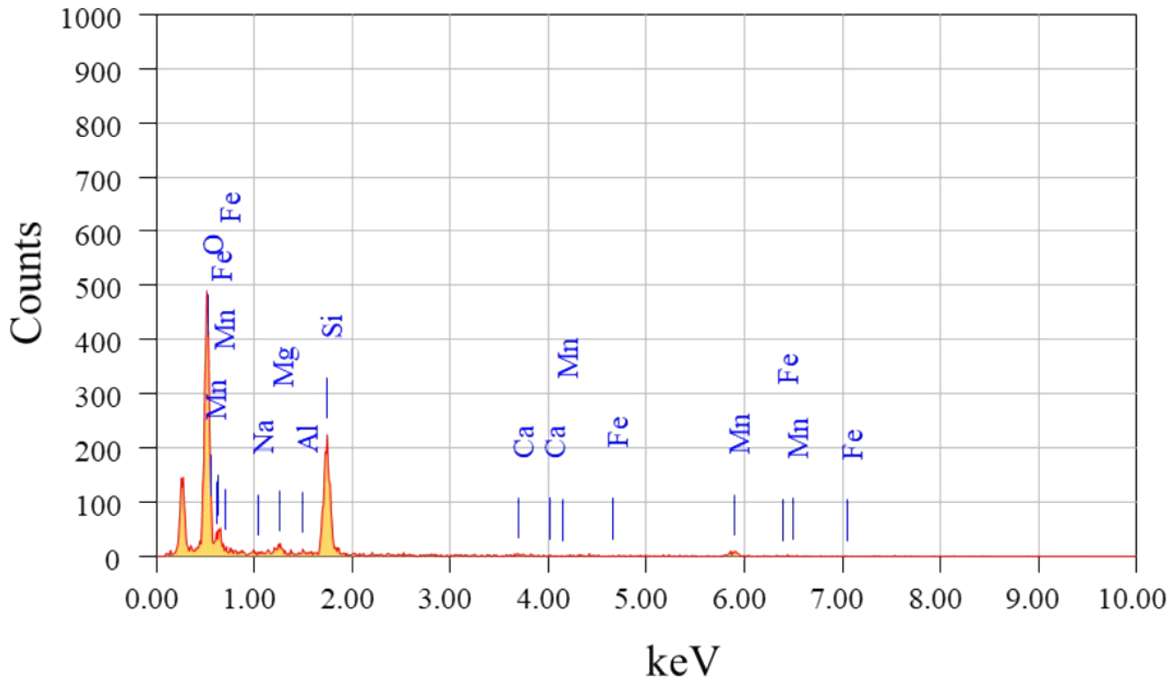

Figure S3. EDS analysis of 2D Rhodonite.

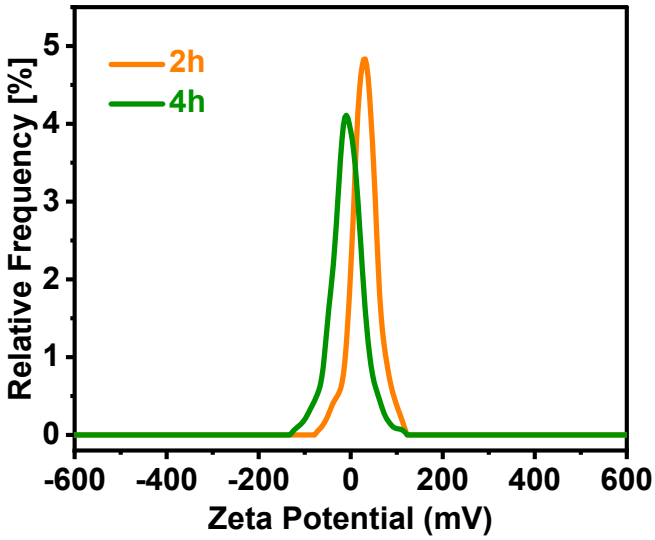

Figure S4. Relative frequency vs Zeta potential plot for 2h, 4h exfoliated Rhodonite

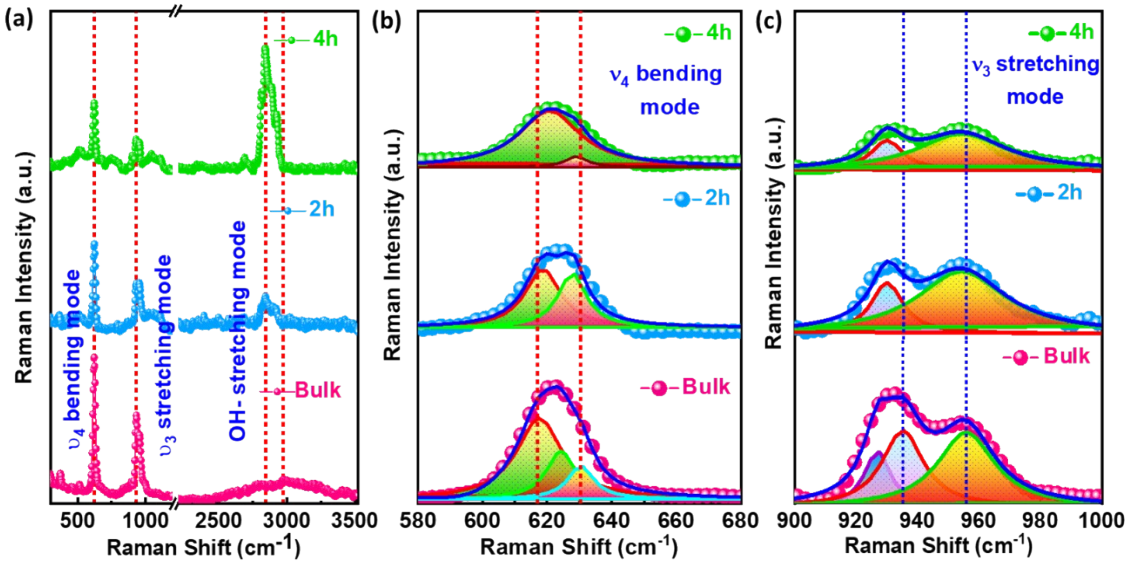

Figure S5. (a) Raman shift for bulk, 2h and 4h exfoliated rhodonite; (b) Deconvolution of the ν_4 bending mode in the Raman spectra of bulk, 2h and 4h exfoliated rhodonite;

(c) Deconvolution of the ν_3 antisymmetric stretching mode for bulk, 2h and 4h exfoliated rhodonite.

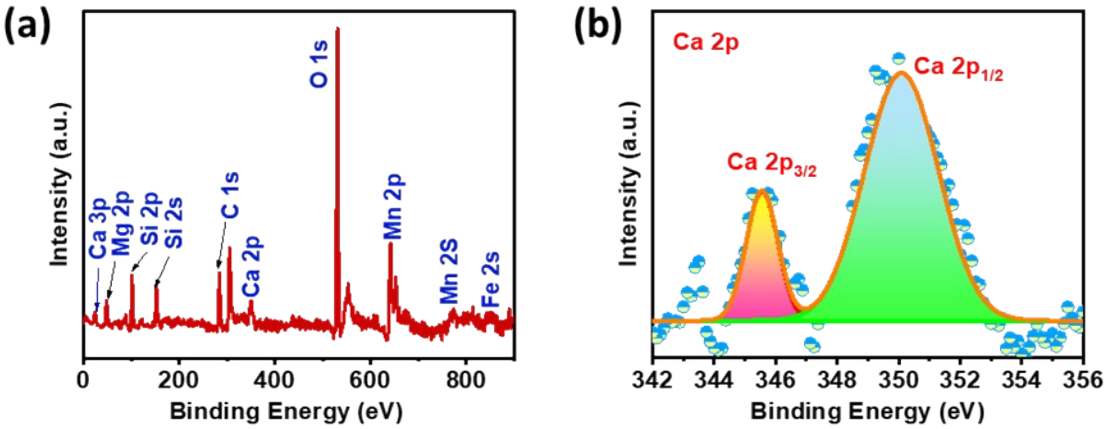

Figure S6. (a) XPS surface scan of the 2D sample; (b) XPS spectra displaying the characteristic peaks of Ca 2p.

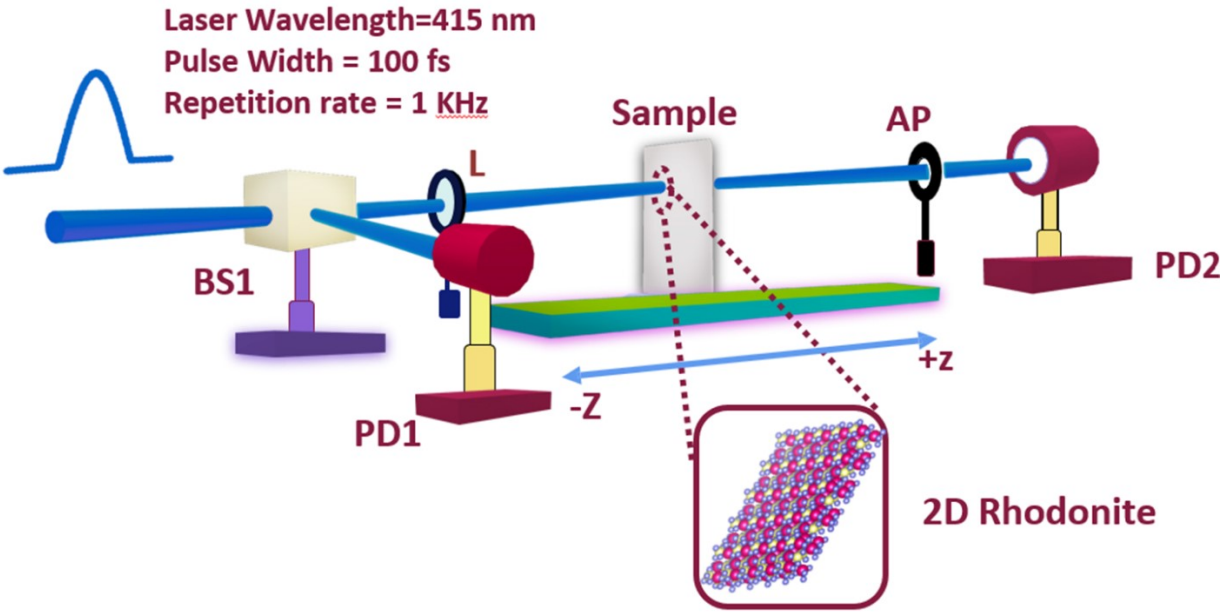

Figure S7. Experimental Z-scan setup: BS1: Beam Splitter; PD1 and PD2: Photodetectors; L: Lens; AP: Aperture.

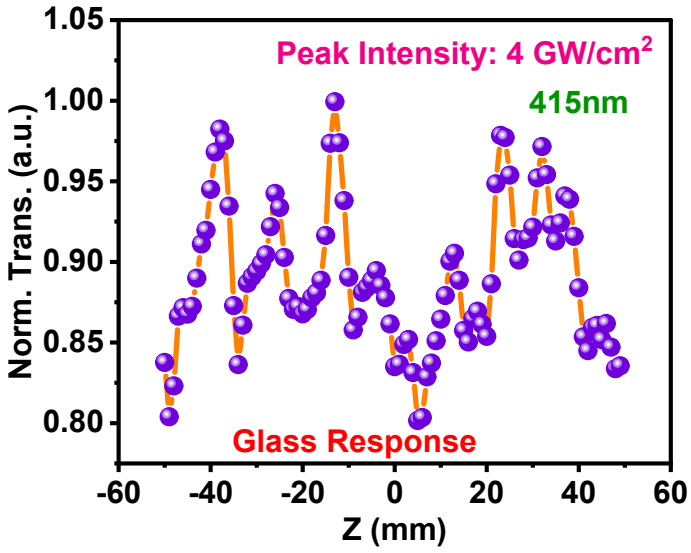

Figure S8. Response of the Glass substrate at peak intensity 4 GW/cm^2 and 415nm wavelength.

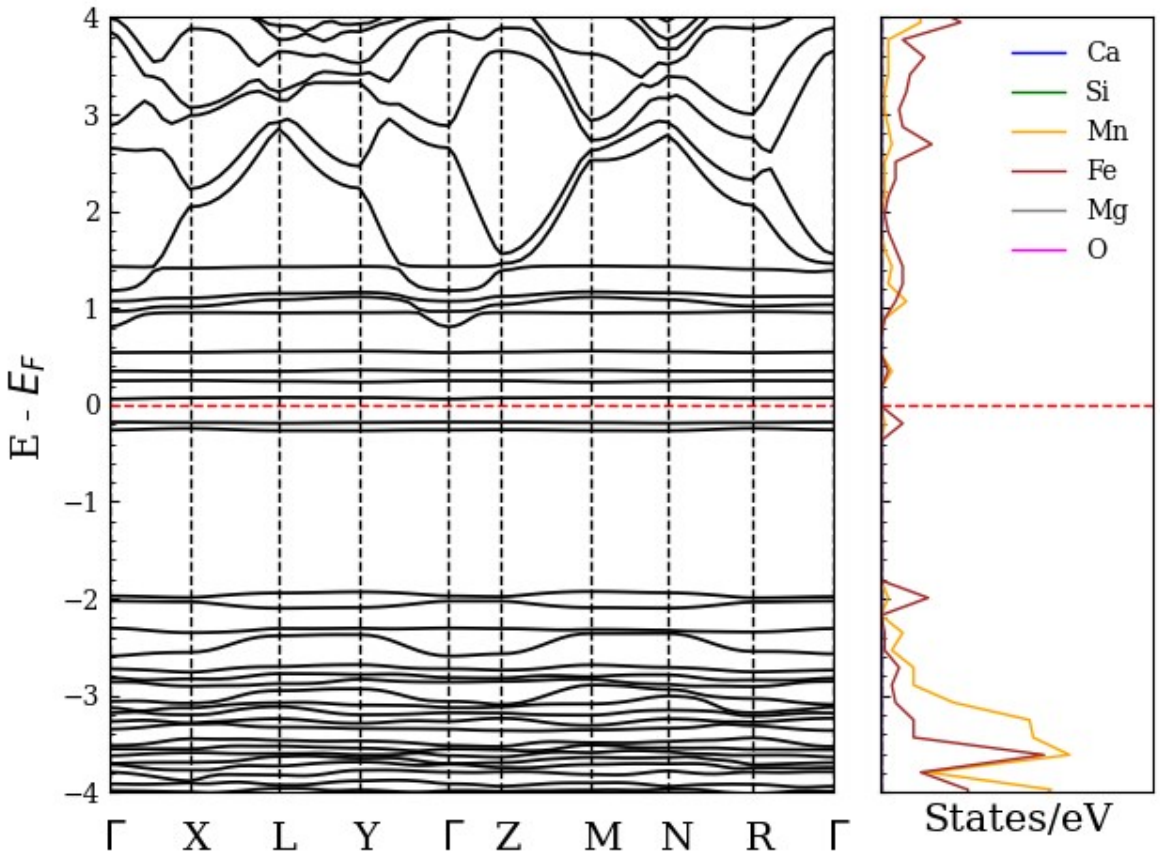

Figure S9: Electronic band structure and projected density of states for bulk rhodonite.

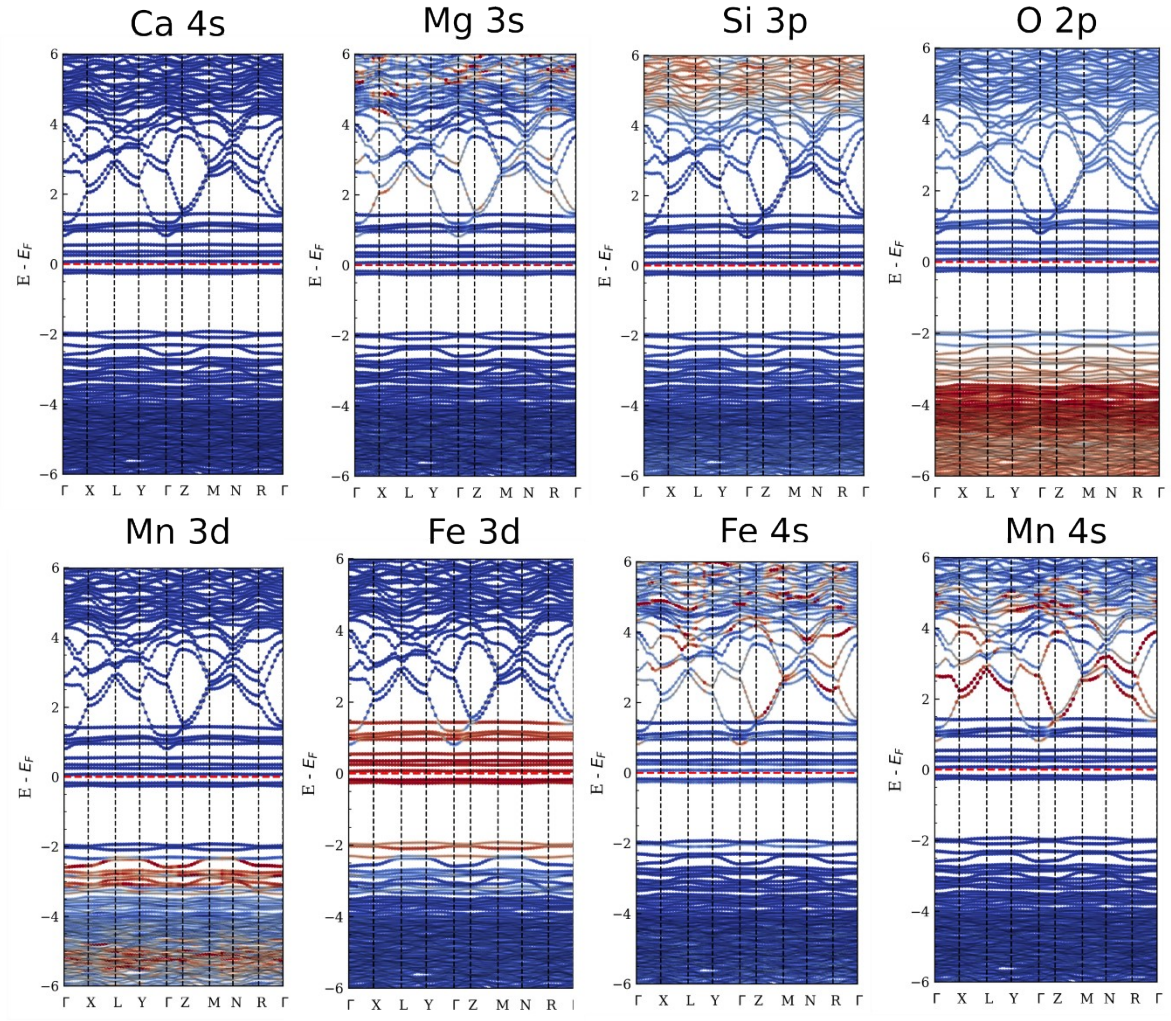

Figure S10: Orbital contributions for electronic structure of bulk rhodonite.

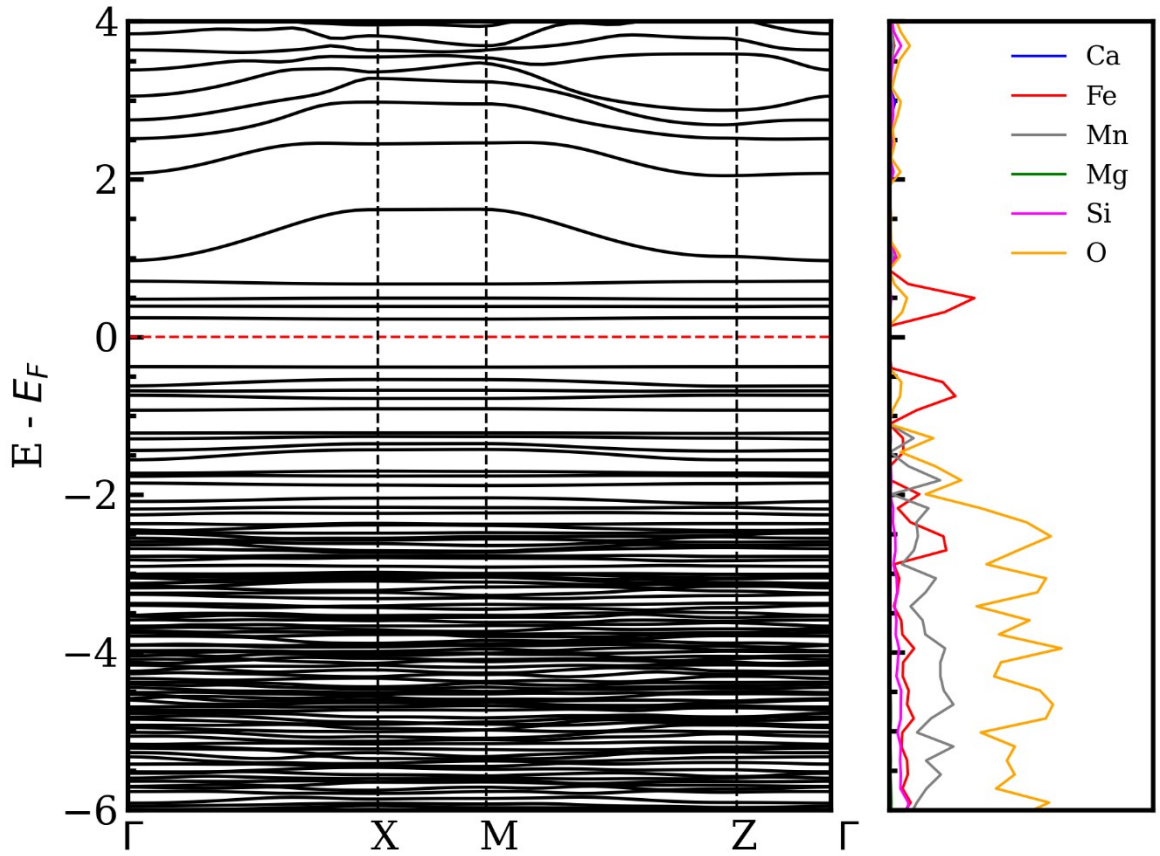

Figure S11: Electronic band structure and projected density of states for 2D rhodonite.

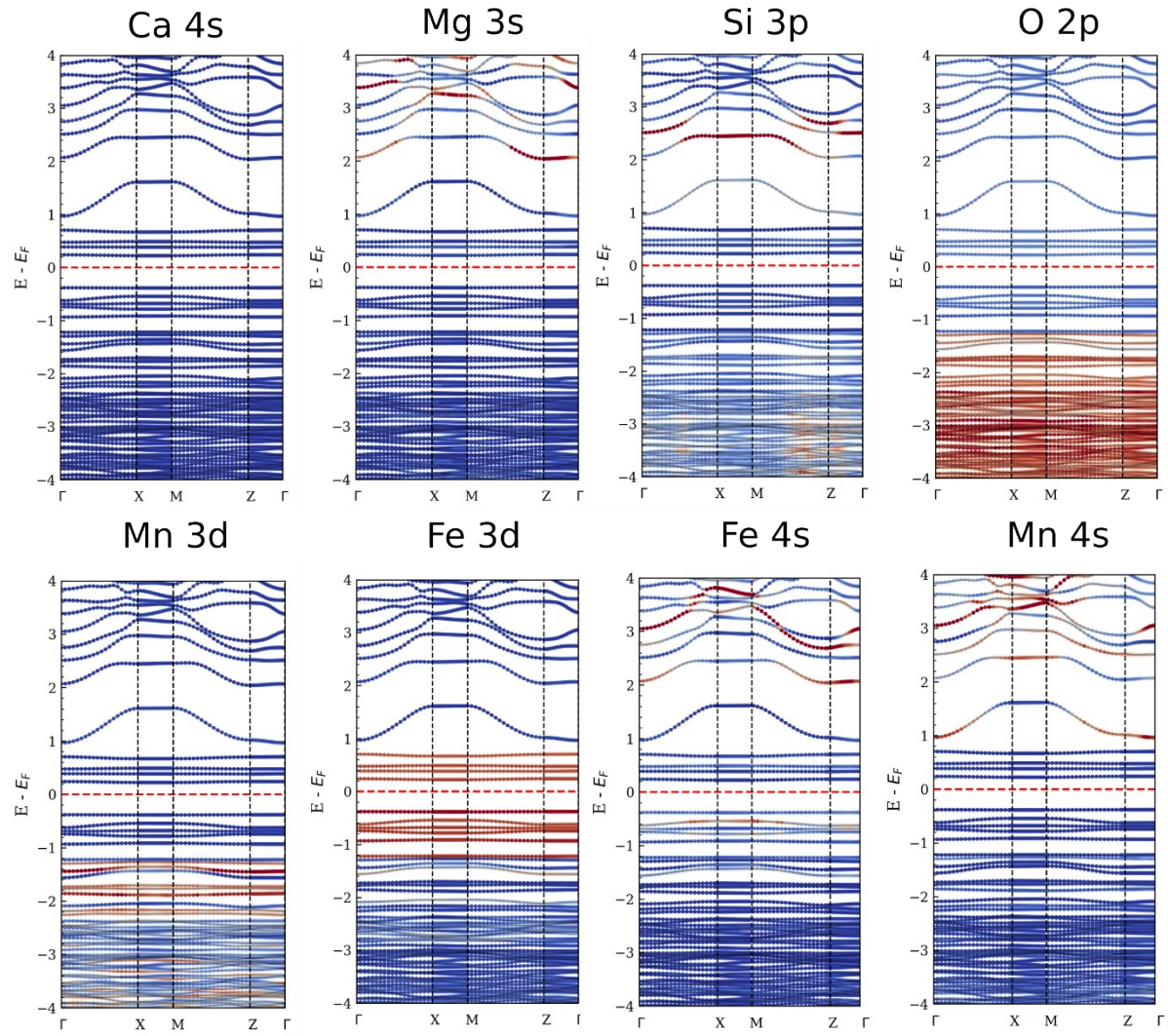

Figure S12: Orbital contributions for electronic structure of 2D rhodonite.

Table S1. TPA coefficients of recently reported materials.

Sample	Laser Pulse width, Repetition rate	Laser Wavelength nm	TPA coefficient β (cm/GW)	Refs
Bilayer Graphene	400 fs, 1 KHz	1100	$(2\pm0.4) \times 10^4$	[1]
Bilayer Graphene	400 fs, 1 KHz	780	$(1\pm0.2) \times 10^4$	[1]
MoS_2 monolayer	340 fs, 1 KHz	1030	$(7.62\pm0.15)\times 10^3$	[2]
WS_2 monolayer	35 fs, 1 KHz	800	1.183×10^3	[3]
2D Bi_2S_3	35 fs, 1 KHz	800	4.25×10^2	[4]
2D Rhodonite	100 fs, 1 KHz	415	9.12×10^4	This work

Table S2. Optical Limiting Threshold values of recently reported materials.

Sample	Laser Wavelength (nm)	Optical Limiting Threshold (mJ/cm^2)	Ref
MoS_2-PMMA Film	1064	315.1	[5]
Single Layer Graphene	532	10	[6]
WS_2 Nanosheets	532	62	[7]
Monolayer Biotite	415	1.51	[8]
2D Rhodonite	415	0.38	This work

References

[1] H. Yang *et al.*, “Giant two-photon absorption in bilayer graphene,” *Nano Lett*, vol. 11, no. 7, pp. 2622–2627, Jul. 2011, doi: 10.1021/nl200587h.

[2] Y. Li *et al.*, “Giant two-photon absorption in monolayer MoS2,” *Laser Photon Rev*, vol. 9, no. 4, pp. 427–434, Jul. 2015, doi: 10.1002/lpor.201500052.

[3] C. Lu *et al.*, “Layer-Dependent Nonlinear Optical Properties of WS2, MoS2, and Bi2S3Films Synthesized by Chemical Vapor Deposition,” *ACS Appl Mater Interfaces*, vol. 14, no. 1, pp. 2390–2400, Jan. 2022, doi: 10.1021/acsami.1c21797.

[4] J. Yu *et al.*, “Giant nonlinear optical activity in two-dimensional palladium diselenide,” *Nat Commun*, vol. 12, no. 1, Dec. 2021, doi: 10.1038/s41467-021-21267-4.

[5] G. Liang *et al.*, “Optical limiting properties of a few-layer MoS 2 /PMMA composite under excitation of ultrafast laser pulses,” *J Mater Chem C Mater*, vol. 7, no. 3, pp. 495–502, 2019, doi: 10.1039/c8tc04200d.

[6] G. K. Lim *et al.*, “Giant broadband nonlinear optical absorption response in dispersed graphene single sheets,” *Nat Photonics*, vol. 5, no. 9, pp. 554–560, Sep. 2011, doi: 10.1038/nphoton.2011.177.

[7] H. Long *et al.*, “Tuning nonlinear optical absorption properties of WS2 nanosheets,” *Nanoscale*, vol. 7, no. 42, pp. 17771–17777, Nov. 2015, doi: 10.1039/c5nr04389a.

[8] D. Mitra *et al.*, “Vacancy-Enhanced Biotite Nanosheets for Optical Limiters,” *ACS Appl Nano Mater*, Apr. 2025, doi: 10.1021/acsanm.5c00454.